

## Nonlinear plastic modes in disordered solids

Luka Gartner and Edan Lerner\*

*Institute for Theoretical Physics, Institute of Physics, University of Amsterdam, Science Park 904, 1098 XH Amsterdam, The Netherlands*

(Received 24 July 2015; published 28 January 2016)

We propose a theoretical framework within which a robust micromechanical definition of precursors to plastic instabilities, often termed soft spots, naturally emerges. They are shown to be collective displacements (modes)  $\hat{z}$  that correspond to local minima of a barrier function  $b(\hat{z})$ , which depends solely on inherent structure information. We demonstrate how some heuristic searches for local minima of  $b(\hat{z})$  can *a priori* detect the locus and geometry of imminent plastic instabilities with remarkable accuracy, at strains as large as  $\gamma_c - \gamma \sim 10^{-2}$  away from the instability strain  $\gamma_c$ . Our findings suggest that the *a priori* detection of the entire field of soft spots can be effectively carried out by a systematic investigation of the landscape of  $b(\hat{z})$ .

DOI: [10.1103/PhysRevE.93.011001](https://doi.org/10.1103/PhysRevE.93.011001)

Plastic flow of disordered solids subjected to external loading is known to occur via localized rearrangements of small sets of particles, coined shear transformations [1]. Such rearrangements have been identified in experiments on bubble rafts [2], foams [3], emulsions [4,5], and colloidal glasses [5,6], as well as in atomistic computer simulations of model glasses [7,8]. An example of such a shear transformation, observed in a model glass in two dimensions deformed under athermal quasistatic shear [9], is displayed in Fig. 1(b). Shear transformations are known to self-organize in spatially correlated patterns [10–16] in solids subjected to large stresses and low deformation rates. Their densities and other statistical properties, and mechanical consequences, are a subject of much recent debate [17–26]. Two questions, central to theoretical descriptions of elastoplasticity, that we address in this work are whether shear transformations can be predicted *a priori* and if so, how.

The micromechanical process in which an athermal disordered solid destabilizes under quasistatic deformation is understood asymptotically close to an instability strain  $\gamma_c$  as a saddle-node bifurcation of the potential energy  $U$  [12,27,28]. The immediate precursors to shear transformations at strains  $\gamma \rightarrow \gamma_c$  are identified as destabilizing eigenfunctions  $\hat{\Psi}_c$  (i.e., their associated eigenvalues vanish at  $\gamma_c$ ) of the dynamical matrix  $\mathcal{M}_{ij} = \frac{\partial^2 U}{\partial \bar{x}_i \partial \bar{x}_j}$ , where  $\bar{x}_i$  denotes the coordinate vector of the  $i$ th particle. Such an eigenfunction is presented in Fig. 1(a) [9]. In the following we refer to such eigenfunctions as destabilizing modes to distinguish them from the postinstability displacements of particles (agglomerations of shear transformations) that can be spatially extended. In Fig. 1(b) we demonstrate that, when the postinstability displacements are not spatially extended, but rather form an isolated elementary shear transformation, their spatial structure is very similar to that of the destabilizing mode. In contrast with the postinstability displacements that depend in general on a specific choice of dynamics [14] and on external control parameters such as temperature [15], strain [11], and strain rate [16], the spatial structure of destabilizing modes is an intrinsic characteristic of the multidimensional potential energy function and is therefore the focus of the present study.

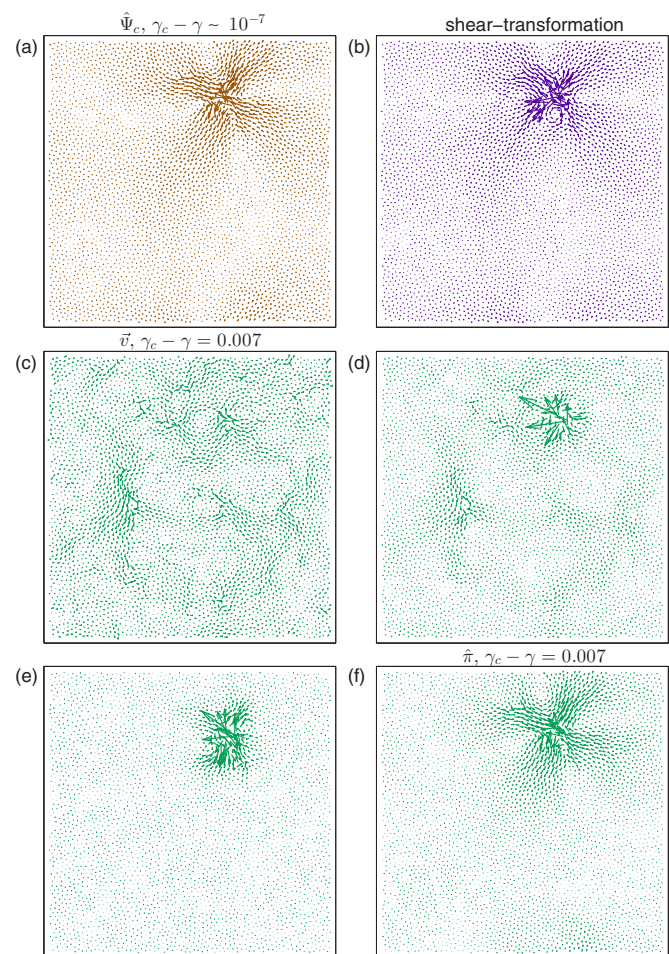


FIG. 1. Plastic instability in a sheared two-dimensional model glass. (a) Destabilizing eigenfunction  $\hat{\Psi}_c$ . (b) Elementary shear transformation: the postinstability displacements that followed the instability of (a). (c) Nonaffine displacements  $\bar{v}$  calculated at  $\delta\gamma \equiv \gamma_c - \gamma = 0.007$ . This delocalized field is used as the initial conditions  $\hat{z}_{\text{ini}}$  for the minimization of  $b(\hat{z})$  (see the main text), the result of which is the plastic mode  $\hat{\pi}$  displayed in (f). (d) and (e) Intermediate states along the minimization of  $b(\hat{z})$ .

A robust mechanical definition of the precursors of plastic instabilities away from instability strains has not yet been put forward. Much effort has been dedicated recently to studying

\*Corresponding author: e.lerner@uva.nl

the role played by low-frequency normal modes in determining these precursors [29–34]. One key difficulty encountered in such studies is that low-frequency plane waves, which have no appreciable effect on plasticity [17], dominate the lower parts of the spectra of conventional model glasses, thus hindering attempts to use low-frequency modes to define flow-defect densities and correlate them with rates of plastic flow.

Another difficulty, which has been largely overlooked in the context of elastoplasticity, is that mere frequencies of normal modes are not indicative of their relevance to plastic processes. In fact, modes that lead to mechanical instabilities (i.e., take the system over energy barriers and into neighboring inherent states) appear as eigenfunctions of the dynamical matrix only very close to plastic instabilities, giving rise to difficulties in their detection and statistical quantification. Here we show that the effective detection of such modes away from plastic instabilities is made possible by accounting for the relevant nonlinearities of the potential energy landscape. We provide a theoretical framework that naturally embeds a micromechanical definition of the precursors to plastic instabilities and that effectively accounts for the said nonlinearities.

We begin the discussion by considering an athermal elastic solid, of  $N$  particles in  $d$  dimensions, and let  $\hat{z}$  denote an  $Nd$ -dimensional unit vector, i.e.,  $\hat{z}_i \cdot \hat{z}_i = 1$ . Here and in what follows repeated indices, labeling particles, are understood to be summed over unless indicated otherwise. The coordinates  $\vec{x}$  are displaced in the direction defined by  $\hat{z}$  according to  $\delta\vec{x} = s\hat{z}$  and we expand the potential energy  $U$  as

$$\delta U_{\hat{z}}(s) \equiv U(s) - U_0 \simeq \frac{1}{2}\kappa_{\hat{z}}s^2 + \frac{1}{6}\tau_{\hat{z}}s^3, \quad (1)$$

where  $U_0$  is the energy of the minimum in which the system resides,  $\kappa_{\hat{z}} \equiv \mathcal{M}_{ij} : \hat{z}_i \hat{z}_j$  is the stiffness associated with  $\hat{z}$ , and  $\tau_{\hat{z}} \equiv \frac{\partial^3 U}{\partial \vec{x}_i \partial \vec{x}_j \partial \vec{x}_k} : \hat{z}_i \hat{z}_j \hat{z}_k$  is referred to in the following as the asymmetry associated with  $\hat{z}$ . Within this cubic expansion, stationary points occur at  $s = 0$  and  $s_* = -2\frac{\kappa_{\hat{z}}}{\tau_{\hat{z}}}$ ;  $s = 0$  corresponds to the minimum in which the system resides, while  $s_*$  represents the saddle point (energy barrier) that separates this minimum and a neighboring inherent state. We thus define the energy difference between these stationary points, within the cubic expansion, as our barrier function

$$b(\hat{z}) \equiv \frac{1}{2}\kappa_{\hat{z}}s_*^2 + \frac{1}{6}\tau_{\hat{z}}s_*^3 = \frac{2\kappa_{\hat{z}}^3}{3\tau_{\hat{z}}^2}. \quad (2)$$

We emphasize that  $b(\hat{z})$  is defined for a particular inherent state of an elastic solid in mechanical equilibrium and is a function of the multidimensional direction  $\hat{z}$ . It has a rough landscape;<sup>1</sup> in this work we focus on directions  $\hat{\pi}$  that correspond to local minima of  $b(\hat{z})$ , i.e., they satisfy  $\frac{\partial b}{\partial \hat{z}_i} |_{\hat{z}=\hat{\pi}} = 0$ , and  $\frac{\partial^2 b}{\partial \hat{z}_i \partial \hat{z}_j} |_{\hat{z}=\hat{\pi}}$  is positive semidefinite. We refer to these directions in what follows as plastic modes. From the definition of  $b(\hat{z})$  it is clear that plastic modes  $\hat{\pi}$  are associated with small stiffnesses  $\kappa_{\hat{\pi}}$  and large asymmetries  $\tau_{\hat{\pi}}$ ; they can be found numerically by minimizing  $b(\hat{z})$  over directions  $\hat{z}$ , starting from some initial direction  $\hat{z}_{\text{ini}}$ , as demonstrated in Figs. 1(c)–1(f). Small  $b(\hat{z})$ 's should appropriately describe

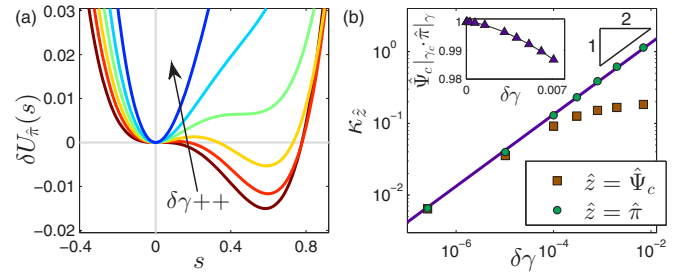


FIG. 2. (a) Variations  $\delta U_{\hat{\pi}}(s)$  of the potential energy upon displacing the particles a distance  $s$  along plastic modes  $\hat{\pi}$ , obtained as described in the text. The curves correspond to  $\delta\gamma = 10^{-5}, 10^{-4}, 3 \times 10^{-4}, 8 \times 10^{-4}, 2 \times 10^{-3}, 7 \times 10^{-3}$ . (b) Stiffnesses  $\kappa_{\hat{z}} = \mathcal{M}_{ij} : \hat{z}_i \hat{z}_j$  associated with the plastic modes  $\hat{\pi}$  used to calculate the variations plotted in (a) (circles) and with the destabilizing eigenfunction  $\hat{\Psi}_c$  vs  $\delta\gamma$  (squares). Inset: overlaps  $\hat{\Psi}_c |_{\gamma_c} \cdot \hat{\pi} |_{\gamma}$  vs  $\delta\gamma$ .

low saddle points (barriers) that separate the system from neighboring inherent states. We therefore expect modes  $\hat{\pi}$  that correspond to low-lying minima of  $b(\hat{z})$  (which are found by cleverly choosing an appropriate  $\hat{z}_{\text{ini}}$  for the minimization) to encode information about imminent plastic instabilities.

This approach is demonstrated in Fig. 1; in Fig. 1(a) we display a destabilizing mode  $\hat{\Psi}_c$  calculated at the first-encountered plastic instability in an athermally sheared model glass, here at a strain  $\gamma_c = 0.011521$ . Prior to this instability, at strains  $\gamma = \gamma_c - \delta\gamma$ , the nonaffine displacement field  $\vec{v}_i \equiv -\mathcal{M}_{ij}^{-1} \cdot \frac{\partial^2 U}{\partial \vec{x}_j \partial \gamma}$  is calculated [27]. An example of  $\vec{v}$ , calculated at  $\delta\gamma = 0.007$ , is shown in Fig. 1(c). At this distance (in strain) from the instability, the nonaffine displacements  $\vec{v}$  are largely delocalized. We use the normalized  $\hat{v} = \vec{v}/\|\vec{v}\|$  as the initial conditions  $\hat{z}_{\text{ini}}$  for the minimization of  $b(\hat{z})$ ; snapshots along the minimization are displayed in Figs. 1(d) and 1(e). Upon convergence, we find a local minimum in the direction  $\hat{\pi}$ , which is displayed in Fig. 1(f). The resemblance between  $\hat{\pi}$  and the destabilizing mode  $\hat{\Psi}_c$  is striking: Both the geometry and the core location appear to agree perfectly. This remarkable agreement is quantified in the inset of Fig. 2(b), where we plot the overlaps  $\hat{\Psi}_c |_{\gamma_c} \cdot \hat{\pi} |_{\gamma}$  as a function of the distance to the instability strain.

The protocol described above is carried out over a broad range of intervals  $\delta\gamma$ , as specified in the caption of Fig. 2. For each  $\delta\gamma$ , after finding  $\hat{\pi}$  as described above, we calculated its associated energy variation  $\delta U_{\hat{\pi}}(s)$  and stiffness  $\kappa_{\hat{\pi}}$ , which are displayed in Figs. 2(a) and 2(b), respectively. In this example, already at a distance of the order  $\delta\gamma \approx 10^{-3}$  to the instability strain, following the plastic mode  $\hat{\pi}$  would carry the system above an energy barrier and into a neighboring minimum.

The resolution of the plastic mode as shown in Fig. 1 uses the nonaffine displacements  $\vec{v}$  as the heuristic guess for  $\hat{z}_{\text{ini}}$ ; this choice is made to demonstrate the usefulness of the framework: Despite the extended character of  $\vec{v}$ , it has a large overlap with the plastic mode  $\hat{\pi}$  and thus resides in the basin of  $\hat{\pi}$  on the landscape of  $b(\hat{z})$ . Obtaining the full field of plastic modes, however, requires using other heuristic  $\hat{z}_{\text{ini}}$ 's, which reside in basins that belong to other plastic modes. We leave the investigation of the optimal heuristics for the detection of the full field of plastic modes for future work.

<sup>1</sup>Finding its global minimum is desirable, but is currently a formidable task; we leave the design of algorithms that can find the global minimum of  $b(\hat{z})$  for future studies.

We also plot in Fig. 2(b) the stiffness  $\kappa_{\hat{\psi}_c}$  associated with the destabilizing mode  $\hat{\psi}_c$ . We find that only very close to the instability ( $\delta\gamma \lesssim 10^{-5}$ ), the scaling  $\kappa_{\hat{\psi}_c} \sim \sqrt{\delta\gamma}$  holds,<sup>2</sup> whereas the stiffness associated with  $\hat{\pi}$  follows  $\kappa_{\hat{\pi}} \sim \sqrt{\delta\gamma}$  up to strains of order 1% away from the instability. This finding supports the robustness of our definition of plastic modes and the usefulness of our framework. It also supports the picture proposed by a number of recent studies [19–24] that assumes that the (reversible) destabilization process of a soft spot in a deformed glass is predominantly coupled to the external load and not to other coexisting (reversible) destabilization processes.

The scaling  $\kappa_{\hat{\pi}} \sim \sqrt{\delta\gamma}$  can be derived as follows. Modes  $\hat{\pi}$  pertain to local minima of  $b(\hat{z})$  and therefore satisfy  $\frac{\partial b}{\partial \hat{z}}|_{\hat{z}=\hat{\pi}} = 0$ , which implies that (see [9])

$$\frac{\partial^3 U}{\partial \hat{x}_i \partial \hat{x}_j \partial \hat{x}_k} : \hat{\pi}_i \hat{\pi}_j \hat{\pi}_k = \frac{\tau_{\hat{\pi}}}{\kappa_{\hat{\pi}}} \mathcal{M}_{ij} \cdot \hat{\pi}_j. \quad (3)$$

Using this relation, we calculate the leading-order variation of the stiffness  $\kappa_{\hat{\pi}}$  with strain as

$$\begin{aligned} \frac{d\kappa_{\hat{\pi}}}{d\gamma} &\simeq \frac{d\mathcal{M}_{ij}}{d\gamma} : \hat{\pi}_i \hat{\pi}_j \simeq \frac{\partial^3 U}{\partial \hat{x}_i \partial \hat{x}_j \partial \hat{x}_k} : \hat{\pi}_i \hat{\pi}_j \hat{v}_k \\ &= -\frac{\tau_{\hat{\pi}}}{\kappa_{\hat{\pi}}} \hat{\pi}_i \cdot \mathcal{M}_{ij} \cdot \mathcal{M}_{jk}^{-1} \cdot \frac{\partial^2 U}{\partial \hat{x}_k \partial \gamma} = -\frac{\tau_{\hat{\pi}}}{\kappa_{\hat{\pi}}} \hat{\pi}_i \cdot \frac{\partial^2 U}{\partial \hat{x}_i \partial \gamma}. \end{aligned} \quad (4)$$

As  $\gamma \rightarrow \gamma_c$ ,  $\kappa_{\hat{\pi}} \rightarrow 0$ , but  $\tau_{\hat{\pi}} \hat{\pi}_i \cdot \frac{\partial^2 U}{\partial \hat{x}_i \partial \gamma}$  goes to a constant, yielding the differential scaling relation  $\frac{d\kappa_{\hat{\pi}}}{d\gamma} \sim -\frac{1}{\kappa_{\hat{\pi}}}$  and thus the observed scaling  $\kappa_{\hat{\pi}} \sim \sqrt{\delta\gamma}$ .

*Comparison to normal modes.* How indicative are normal modes of imminent plastic instabilities, compared to plastic modes? In Fig. 3(a) we present a scatter plot of the barrier function evaluated at normal modes  $\hat{\psi}_\omega$  vs the square of their associated frequencies  $\omega^2$ , calculated for a few tens of undeformed (isotropic) solid realizations. A clear trend appears: Smaller values of  $b(\hat{\psi}_\omega)$  are found for lower-frequency modes. The circled data point represents the mode  $\hat{\psi}_{\min}$  associated with the lowest value of  $b(\hat{\psi}_\omega)$  among all modes calculated; it is displayed in Fig. 3(d). Remarkably, this normal mode displays the same spatial features as observed for destabilizing modes, reinforcing that  $b(\hat{z})$  is indeed sensitive to plasticlike modes. The variation  $\delta U_{\hat{\psi}_{\min}}(s)$  is plotted in Fig. 3(b) (solid line). Despite possessing the smallest  $b$  among our entire ensemble of modes,  $\delta U_{\hat{\psi}_{\min}}(s)$  displays only a slight asymmetry between positive and negative displacements  $s$  and the energy monotonically increases with  $|s|$ . Using  $\hat{\psi}_{\min}$  as the initial condition  $\hat{z}_{\text{ini}}$  for the minimization of  $b(\hat{z})$ , we find the plastic mode  $\hat{\pi}$  displayed in Fig. 3(e). On the face of it,  $\hat{\psi}_{\min}$  and  $\hat{\pi}$  appear to be very similar in their spatial structure and geometry. However, examining the corresponding variation  $\delta U_{\hat{\pi}}(s)$ , represented by the dashed line in Fig. 3(b), reveals a dramatic difference between them: Following  $\hat{\pi}$  takes the system over a energy barrier to a neighboring minimum.

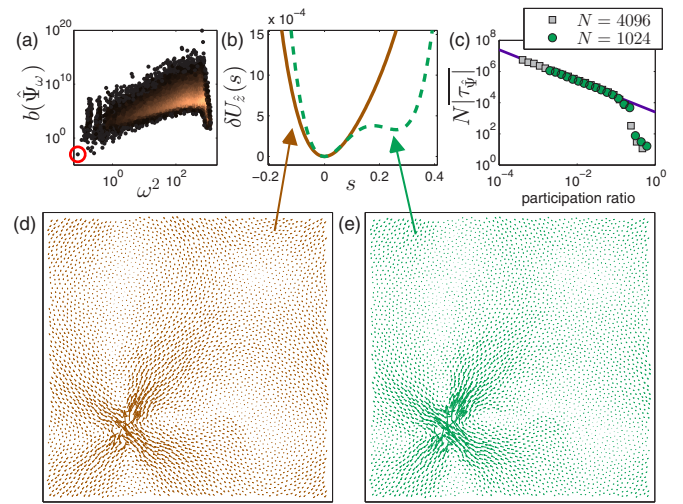


FIG. 3. (a) Scatter plot of the barrier function (2) evaluated for eigenfunctions  $\hat{\psi}_\omega$  of  $\mathcal{M}$  vs their eigenvalues  $\omega^2$ . The eigenfunction  $\hat{\psi}_{\min}$  represented by the circled data point is plotted in (d) and is used as the initial conditions  $\hat{z}_{\text{ini}}$  for the minimization of the barrier function  $b(\hat{z})$ ; the resulting plastic mode  $\hat{\pi}$  is displayed in (e). (b) Variations  $\delta U_{\hat{z}}(s)$ , calculated by displacing the particles according to  $\delta \hat{x} = s \hat{\psi}_{\min}$  (solid curve) and by  $\delta \hat{x} = s \hat{\pi}$  (dashed curve). (c) Products  $N|\tau_{\hat{\psi}}|$ , averaged over bins of the participation ratio; see the text for definitions.

We further utilize our ensemble of normal modes to study the relation between the degree of localization of modes and their associated asymmetries  $\tau_{\hat{\psi}}$ . A similar analysis was carried out in [33] in the context of the unjamming point [35–37]. We quantify the degree of localization of a mode  $\hat{\psi}$  via its participation ratio  $e = [N \sum_i (\hat{\psi}_i \cdot \hat{\psi}_i)^2]^{-1}$ ; localized modes have  $e \sim N^{-1}$ , whereas maximally delocalized modes have  $e \sim 1$ . In Fig. 3(c) we plot the means  $|\tau_{\hat{\psi}}|$ ,<sup>3</sup> averaged over modes  $\hat{\psi}$  with similar participation ratios, for systems of  $N = 1024$  and  $4096$ . We find that for participation ratios  $e < 10^{-1}$ , the asymmetries follow  $|\tau_{\hat{\psi}}| \sim (eN)^{-1}$ . This can be explained with the following simple model: If there are effectively  $N^\alpha$  nonzero components in a normal mode ( $0 < \alpha < 1$ ), normalization then requires that a characteristic nonzero component is of magnitude  $\|\hat{\psi}_i\| \sim N^{-\alpha/2}$ . The participation ratio is then expected to follow  $e \sim N^{\alpha-1}$  (due to summing over positive terms). Since the pairwise potential is short ranged and the tensor elements  $\frac{\partial^3 U}{\partial \hat{x}_i \partial \hat{x}_j \partial \hat{x}_k}$  are of either sign, then  $\tau_{\hat{\psi}}$  consist of a sum over  $N^\alpha$  terms, each of order  $\|\hat{\psi}_i\|^3 \sim N^{-3\alpha/2}$ , of random signs and we therefore expect  $\tau_{\hat{\psi}} \sim N^{-\alpha} \sim (eN)^{-1}$ , in consistency with our measurement. For participation ratios  $e > 10^{-1}$ , this relation breaks down and asymmetries are much smaller than what is predicted by this simple model, which assumes that normal modes are random objects. Nevertheless, the same trend remains unchanged: Delocalized modes are associated, on average, with more

<sup>2</sup>In a system of linear size  $L$ , the scaling law  $\kappa_{\hat{\psi}} \sim \sqrt{\delta\gamma}$  is only expected to hold below  $\delta\gamma \sim L^{-4}$  due to hybridizations with low-frequency plane waves.

<sup>3</sup>We consider the absolute magnitudes  $|\tau_{\hat{\psi}}|$  since normal modes  $\hat{\psi}$ , and therefore also their associated asymmetries  $\tau_{\hat{\psi}}$ , are defined up to a sign.

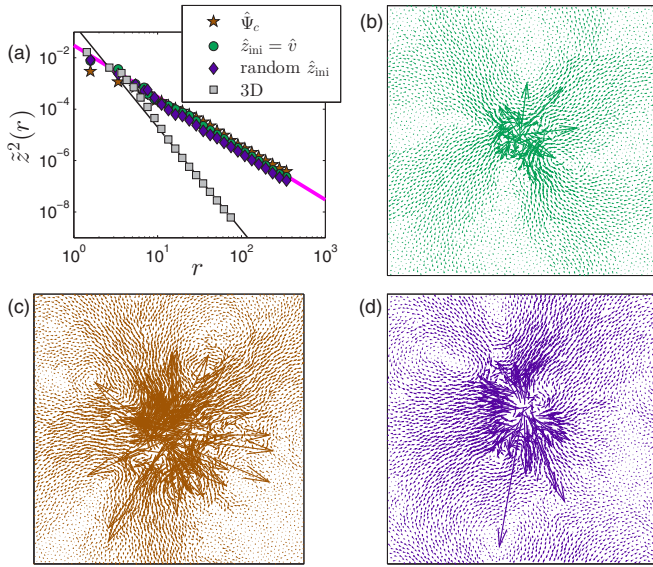


FIG. 4. (a) Spatial decay of plastic modes; see the text for definitions. All modes analyzed decay as  $r^{1-d}$ , as indicated by the solid lines, where  $r$  is the distance to the core center. (b) Plastic mode found by choosing a random  $\hat{z}_{\text{ini}}$ . (c) Plastic mode calculated in a disordered network of relaxed Hookean springs. (d) Plastic mode found in a Lennard-Jones glass under isotropic tension.

symmetric variations of the energy. These observations explain the localized nature of plastic instabilities found in deformed glasses, as can be seen, e.g., in Fig. 1(a).

*Structure of plastic modes.* To characterize the spatial structure of plastic modes, we define  $\hat{z}^2(r)$  as the median of the squared magnitude of the components  $\hat{z}_i \cdot \hat{z}_i$  (no summation implied), taken over a shell of thickness on the order of the nearest-neighbor distance, and of radius  $r$  away from the core of the plastic mode (detecting the locus of the core is explained in [9]). In Fig. 4(a) we compare the spatial decay of two plastic modes, one obtained by setting  $\hat{z}_{\text{ini}}$  to be the direction of the nonaffine displacements (see the definition above and Fig. 1) and the other by setting  $\hat{z}_{\text{ini}}$  to be a random direction. These decay profiles are also compared to that of a destabilizing mode  $\hat{\Psi}_c$ . We also show the decay profile of a plastic mode calculated in a three-dimensional solid. We find that at distances  $r$  away from the core, plastic modes decay as  $r^{1-d}$ . Remarkably, this is the same decay law found for the linear responses of displacements to dipolar point forces [25,38].

In Fig. 4(b) we present a plastic mode obtained with a random  $\hat{z}_{\text{ini}}$ . We find that this mode shares the same geometric features as the destabilizing modes  $\hat{\Psi}_c$  upon shear-induced plastic instabilities: a disordered core and a long-ranged affine quadrupolar shearlike displacement field away from the core [12,25,27]. We thus conclude that plastic modes  $\hat{\pi}$  associated with different local minima of  $b(\hat{z})$  share similar structural features that do not depend on the particular minima to which they correspond.

We finally examine how the geometry of plastic modes depends on the loading conditions imposed on the solid. In Figs. 4(c) and 4(d) two additional examples of plastic modes  $\hat{\pi}$  obtained from a random  $\hat{z}_{\text{ini}}$  are displayed;  $\hat{\pi}$  of Fig. 4(c) was calculated in a disordered network of relaxed Hookean

springs (all springs are neither stretched nor compressed) with an average of 4.1 springs connected to each node. It displays a similar spatial structure as that of plastic modes found in model glasses that are prestressed, i.e., in which finite forces are exerted between the constituent particles [39]. Our findings indicate that proximity to prestress-induced micromechanical buckling instabilities [40] is not the origin of the generic structure of plastic modes.

The plastic mode  $\hat{\pi}$  of Fig. 4(d) was calculated in a Lennard-Jones glass (with a pairwise potential that includes an attractive term; see [9] for details) under isotropic tension, just before macroscopic failure (here  $-p/B \approx 10^{-2}$  is at least 80% of the yield strain, where  $p$  is the pressure and  $B$  is the bulk modulus). We find in this case that in addition to the clear shearlike displacements that are typically seen in plastic modes found in glasses under compressive stresses, the dilatant part of the displacements due to the tensile loading conditions is apparent. We conclude that the loading conditions imposed on a solid can be reflected in the geometric features of its plastic modes; we leave the systematic study of this dependence for future work.

*Discussion.* In this work we demonstrated that modes  $\hat{\pi}$  corresponding to local minima of the barrier function  $b(\hat{z})$ , coined plastic modes, are indicative of directions in configuration space that lead to plastic instabilities and more so compared to the most localized low-frequency normal modes. As such, our framework can serve as a solid basis for instability-detection algorithms. Such algorithms are highly desirable, as they can put to test theoretical frameworks of elastoplasticity that involve the dynamics of a population of soft spots. These algorithms need not be restricted to the investigation of plastic flow in disordered solids; the generality of our framework would render them suitable for studying a diverse set of systems, including dislocated crystalline solids, deeply supercooled liquids, and proteins.

Furthermore, our theoretical framework explains the origin of the localized nature of plastic instabilities. Building on our framework, we predict that the stiffness associated with plastic modes follows  $\kappa \sim \sqrt{\gamma_c - \gamma}$  and show numerically that this scaling holds over a large range of strains away from an instability strain  $\gamma_c$ . This adds relevance to recently proposed models that assume that reversible destabilization processes of soft spots are decoupled from each other. Finally, we have investigated the spatial features of plastic modes and provided evidence that the detailed geometry of plastic modes is sensitive to the loading conditions imposed on the solid.

Our approach demonstrates the usefulness of the concept of exploring the direction space associated with an inherent state of a solid as a means of extracting micromechanical information that is highly relevant to nonlinear flow processes. Similar approaches could likely be applied towards studying mechanical instabilities in, e.g., granular solids [41] and towards studying other classes of low-energy excitations in glassy solids, e.g., two-level systems [42,43].

We thank Eran Bouchbinder, Smarjit Karmakar, Gustavo Düring, Itamar Procaccia, and Matthieu Wyart for fruitful discussions. This research was funded by the Amsterdam Academic Alliance fellowship of the University of Amsterdam and the Vrije Universiteit Amsterdam.

- [1] A. Argon, *Acta Metall.* **27**, 47 (1979).
- [2] A. S. Argon and H. Kuo, *Mater. Sci. Eng.* **39**, 101 (1979).
- [3] M. Dennin, *Phys. Rev. E* **70**, 041406 (2004).
- [4] P. Hébraud, F. Lequeux, J. P. Munch, and D. J. Pine, *Phys. Rev. Lett.* **78**, 4657 (1997).
- [5] J. Clara-Rahola, T. A. Brzinski, D. Semwogerere, K. Feitosa, J. C. Crocker, J. Sato, V. Breedveld, and E. R. Weeks, *Phys. Rev. E* **91**, 010301 (2015).
- [6] V. Chikkadi, G. Wegdam, D. Bonn, B. Nienhuis, and P. Schall, *Phys. Rev. Lett.* **107**, 198303 (2011).
- [7] D. Deng, A. S. Argon, and S. Yip, *Philos. Trans. R. Soc. London A* **329**, 613 (1989).
- [8] M. L. Falk and J. S. Langer, *Phys. Rev. E* **57**, 7192 (1998).
- [9] See Supplemental Material at <http://link.aps.org/supplemental/10.1103/PhysRevE.93.011001> for details about the models, units, and numerical methods used in this work.
- [10] C. Maloney and A. Lemaître, *Phys. Rev. Lett.* **93**, 016001 (2004).
- [11] A. Tanguy, F. Leonforte, and J.-L. Barrat, *Eur. Phys. J. E* **20**, 355 (2006).
- [12] C. E. Maloney and A. Lemaître, *Phys. Rev. E* **74**, 016118 (2006).
- [13] S. Karmakar, E. Lerner, and I. Procaccia, *Phys. Rev. E* **82**, 055103(R) (2010).
- [14] K. M. Salerno, C. E. Maloney, and M. O. Robbins, *Phys. Rev. Lett.* **109**, 105703 (2012).
- [15] J. Chattoraj and A. Lemaître, *Phys. Rev. Lett.* **111**, 066001 (2013).
- [16] A. Lemaître and C. Caroli, *Phys. Rev. Lett.* **103**, 065501 (2009).
- [17] H. G. E. Hentschel, S. Karmakar, E. Lerner, and I. Procaccia, *Phys. Rev. E* **83**, 061101 (2011).
- [18] E. Bouchbinder and J. S. Langer, *Phys. Rev. Lett.* **106**, 148301 (2011).
- [19] J.-C. Baret, D. Vandembroucq, and S. Roux, *Phys. Rev. Lett.* **89**, 195506 (2002).
- [20] G. Picard, A. Ajdari, F. Lequeux, and L. Bocquet, *Phys. Rev. E* **71**, 010501 (2005).
- [21] M. Talamali, V. Petäjä, D. Vandembroucq, and S. Roux, *Phys. Rev. E* **84**, 016115 (2011).
- [22] J. Lin, A. Saade, E. Lerner, A. Rosso, and M. Wyart, *Europhys. Lett.* **105**, 26003 (2014).
- [23] J. Lin, E. Lerner, A. Rosso, and M. Wyart, *Proc. Natl. Acad. Sci. USA* **111**, 14382 (2014).
- [24] J. Lin and M. Wyart, [arXiv:1506.03639](https://arxiv.org/abs/1506.03639) [*Phys. Rev. X* (to be published)].
- [25] G. Picard, A. Ajdari, F. Lequeux, and L. Bocquet, *Eur. Phys. J. E* **15**, 371 (2004).
- [26] F. Puosi, J. Rottler, and J.-L. Barrat, *Phys. Rev. E* **89**, 042302 (2014).
- [27] C. Maloney and A. Lemaître, *Phys. Rev. Lett.* **93**, 195501 (2004).
- [28] D. L. Malandro and D. J. Lacks, *J. Chem. Phys.* **110**, 4593 (1999).
- [29] A. Tanguy, B. Mantsi, and M. Tsamados, *Europhys. Lett.* **90**, 16004 (2010).
- [30] M. L. Manning and A. J. Liu, *Phys. Rev. Lett.* **107**, 108302 (2011).
- [31] J. Rottler, S. S. Schoenholz, and A. J. Liu, *Phys. Rev. E* **89**, 042304 (2014).
- [32] S. Wijtmans and M. L. Manning, [arXiv:1502.00685](https://arxiv.org/abs/1502.00685).
- [33] N. Xu, V. Vitelli, A. J. Liu, and S. R. Nagel, *Europhys. Lett.* **90**, 56001 (2010).
- [34] M. Mosayebi, P. Ilg, A. Widmer-Cooper, and E. Del Gado, *Phys. Rev. Lett.* **112**, 105503 (2014).
- [35] C. S. O'Hern, L. E. Silbert, A. J. Liu, and S. R. Nagel, *Phys. Rev. E* **68**, 011306 (2003).
- [36] A. J. Liu and S. R. Nagel, *Annu. Rev. Condens. Matter Phys.* **1**, 347 (2010).
- [37] M. van Hecke, *J. Phys.: Condens. Matter* **22**, 033101 (2010).
- [38] E. Lerner, E. DeGiuli, G. Düring, and M. Wyart, *Soft Matter* **10**, 5085 (2014).
- [39] Prestress is a generic feature of glassy solids; see, e.g., S. Alexander, *Phys. Rep.* **296**, 65 (1998).
- [40] M. Wyart, L. E. Silbert, S. R. Nagel, and T. A. Witten, *Phys. Rev. E* **72**, 051306 (2005).
- [41] E. Lerner, G. Düring, and M. Wyart, *Soft Matter* **9**, 8252 (2013).
- [42] P. W. Anderson, B. I. Halperin, and C. M. Varma, *Philos. Mag.* **25**, 1 (1972).
- [43] W. Phillips, *J. Low Temp. Phys.* **7**, 351 (1972).